Impact of DC-link Voltage Ripple on Induction Motor Drives Utilizing Cascaded H-bridge Multilevel Inverter

Adisorn Jewsubpong, **Nattapong Pothi**†,
Chawasak Rakpenthai, and **Jonglak Pahasa**, Non-members

ABSTRACT

This article investigates the impact of DC-link voltage ripple on the performance of the 5-level cascade H-bridge induction motor drive, especially focusing on torque ripple and speed variations. Each H-bridge cell of the inverter obtains an isolated DC power supply from a single-phase full-bridge rectifier. Certain capacitance values are utilized on the output side of rectifiers to visibly demonstrate the different amounts of ripple in the DC-link voltage. In this study, the motor speed is consistently held at 500 rpm throughout the operating range, while the load torque is considered in both no-load and with-load conditions. The in-phase disposition level-shifted technique is employed to produce the switching signals of the 5-level cascade H-bridge induction motor drive based on the indirect-rotor field-oriented control strategy. The validation of the drive system performance influenced by the quality of the DC-link voltage waveform is verified by simulation results.

Keywords: DC-link voltage ripple, Multilevel inverter, Cascaded H-bridge, Induction motor drive, Torque ripple

1. INTRODUCTION

Cascade H-bridge (CHB) multilevel inverters have gained prominence in medium-voltage and high-power motor drive systems due to their low harmonic distortion, fault tolerance, modular design, and capability to produce high-quality output voltage waveforms [1]-[3]. Besides, the switching frequency in the CHB multilevel inverter is generally set lower than that of a typical two-level voltage source inverter (VSI), resulting in a considerable reduction in switching losses [4]-[6]. Therefore, the CHB multilevel inverter is extensively utilized across various applications, such as medium-voltage motor drives, renewable energy sources, high-voltage transmission systems, photovoltaic power generation system, and electric vehicles (EVs) [7], [8], [9]. Furthermore, induction motors (IMs) commonly operate with the CHB multilevel inverter across numerous fields due to their advantages, and they are of interest for application in EVs and hybrid EVs. However, minimizing torque ripple and speed fluctuations remains a priority [9], [10].

In medium-voltage CHB IM drives, an isolated step-down transformer in consort with a diode bridge rectifier is commonly required because it provides an appropriate voltage level for IM drives and isolates the DC sources in each H-bridge cell which can mitigate dominant harmonics [6]. The primary trend to consider is the reduction of DC-link capacitance in the H-bridge cell and the optimization of power switches [11]. The regenerative CHB topology is introduced in [12] to produce the DC source for the CHB multilevel inverter using the PWM rectifier configuration, which is called the active front end (AFE), instead of the diode bridge rectifier. This approach utilizes closed-loop voltage ripple regulator to reduce the active capacitance by around 25 percent, and it has been improved to diminish further passive filters [13]. Likewise, the CHB topology-based the static synchronous compensator (CHB-StatCom) is presented in [14] to reduce the capacitance. It employs the measured DC-link voltage and reactive power to switch the AFE rectifiers. Based on this method, the lifespan and reliability of capacitors may diminish under conditions of high voltage ripple [11]. Although AFE rectifier topology recovers energy in some specific situations, for instance, downhill belt conveyors, it requires a larger footprint and a more efficient heatsink design, which results in higher costs compared to the diode bridge rectifier [8]. In [15], the half-bridge inverter is utilized instead of the full-bridge inverter in H-bridge cells to reduce the quantity of power switches, whereas the DC power supply is generated by the AFE rectifier. However, the quality of the DC-link voltage waveform would be meticulously evaluated, particularly under load conditions. Moreover, fluctuations in the DC-link voltage represent a serious concern that can adversely impact the performance of motor drives. In [16] the impact of DC-link voltage ripples on the motor drive performance is investigated, focused mainly on spectral analysis, while the supercapacitor is utilized to reduce the DC-link voltage fluctuations [17]. Although numerous studies examine

Manuscript received on June 13, 2025; revised on September 1, 2025; accepted on September 30, 2025. This paper was recommended by Associate Editor Chainarin Ekkaravarodome.

The authors are with Department of Electrical Engineering, School of Engineering, University of Phayao, Phayao, Thailand.

†Corresponding author: nattapong.po@up.ac.th

Digital Object Identifier: 10.37936/ecti-eec.2525233.259532

the effects of DC-link voltage fluctuations on the drive system performance, few examine the consequences on the torque ripple and speed variations.

A major advantage of the CHB multilevel inverter is its capacity to proportionally increase the output voltage in accordance with its voltage levels and its ability to provide low total harmonic distortion compared with usual 2-level inverters [18]. Residences, agricultural applications, and small enterprises can commonly obtain a single-phase AC power supply, while three-phase AC motors are required for specific applications. It is noted that the 5-level CHB inverter with a step-down single-phase transformer (2:1) in the rectifier part of H-bridge cell can provide an adequate level of output voltage to drive three-phase AC motors.

In this paper, the impact of the DC-link voltage ripple on the 5-level CHB IM drive performance, which focuses on the torque ripple and speed fluctuations under no-load and load conditions, is proposed. Employing varied values of capacitance on the output side of the full-bridge diode rectifier generates various levels of ripple in the DC-link voltage. The influence of the DC-link voltage ripple on the IM drive performance is confirmed by simulation results.

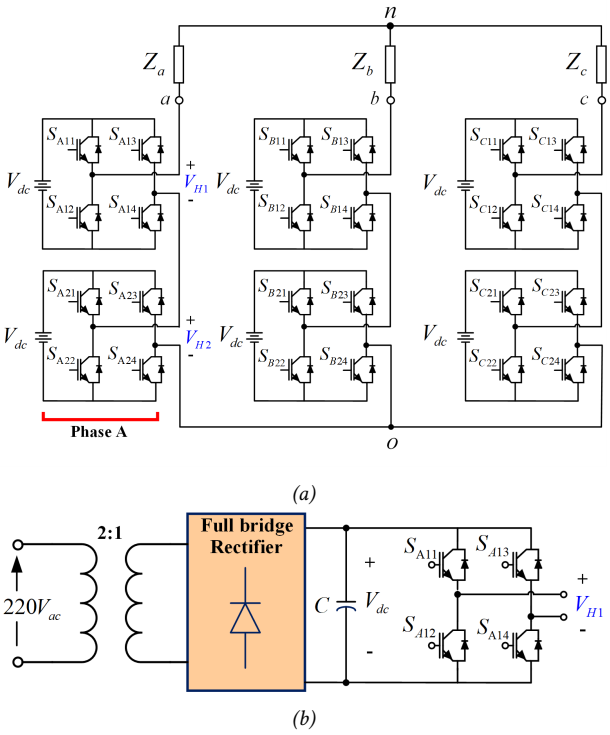

***Fig. 1**: CHB Multilevel Inverter Configuration.*

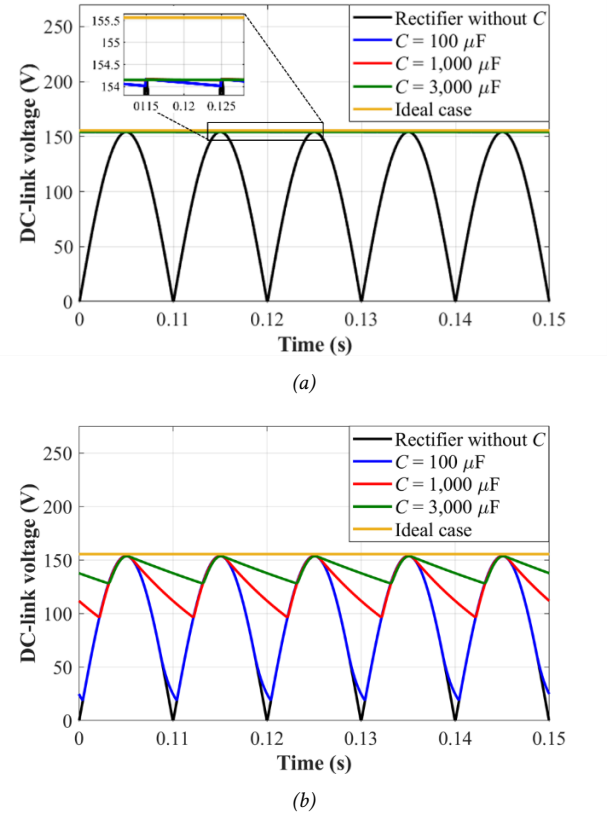

***Fig. 2**: DC-link Voltage Waveforms.*

2. CHB MULTILEVEL INVERTER

2.1 Topology and Operation

The CHB multilevel inverter comprises several H-bridge cell units arranged in series within each phase, i.e., the 5-level CHB inverter arrangement depicted in Fig. 1(a). Indeed, the output voltage can be increased in proportion to the number of CHB voltage levels, which is equivalent to the total number of H-bridge cells [2], as given by (1). The whole number of active switches utilized in the CHB inverter can be defined by (2).

$$m = 2H + 1 \tag{1}$$

$$N_{sw} = 6\,(m - 1) \tag{2}$$

where m is the number of CHB voltage levels, H denotes the total number of H-bridge cells in each phase, and Nsw is the whole number of switches.

In Fig. 1(a), the inverter phase voltage can be determined by (3) based on the series of the top and bottom H-bridge cells.

$$V_{ao} = V_{H1} + V_{H2} \tag{3}$$

where V_{ao} represents the inverter phase voltage in phase A relative to the inverter neutral point o, and V_{H1}, V_{H2} indicate the output voltages of the top and bottom H-bridge cells, respectively.

Fig. 1 illustrates the CHB multilevel inverter topology employed in this study to evaluate the effects of DC-link voltage ripple. The single-phase full-bridge diode rectifier, equipped with an isolated step-down transformer on the input side as shown in Fig. 1(b), provides an independent DC-link voltage for the 5-level CHB inverter. Because of the crucial merit of such an inverter, i.e., raising the output voltage level, it is capable of delivering adequate output voltage for three-

phase IM drives with a single-phase AC supply, which offers simplicity and accessibility in several applications. Furthermore, the step-down transformer can double the available current for the CHB-IM drive. Indeed, the capacitor is often used to reduce the fluctuations in the output voltage of the rectifier, which can directly affect the quality of the DC-link voltage waveform in the inverter. Consequently, the selection of an appropriate capacitance for the inverter is significant, particularly in the CHB-IM drive system. Fig. 2 shows a comparison of the simulation results for the DC-link voltage waveforms generated by the single-phase full-bridge rectifier under both no-load and load conditions, as illustrated in Fig. 2(a), and Fig. 2(b), respectively. The capacitance values of 100 μF, 1,000 μF, and 3,000 μF are compared with no capacitor and the ideal case. In the no-load condition, as indicated in Fig. 2(a), the DC-link voltage ripple remains quite consistent across all capacitance values, close to the ideal case.

This simulation incorporates the threshold voltage and internal resistance of each diode rectifier, definitely 0.7 V and 0.02 Ω. Under the load condition, where the load current is approximately 10 A as expressed in Fig. 1(b), the increased capacitance values result in a reduced DC-link voltage ripple.

2.2 Switching Signal Generation

Pulse width modulation (PWM) techniques for CHB multilevel inverters can be commonly categorized into two techniques, i.e., phase-shifted and level-shifted modulation techniques. Moreover, the level-shifted modulation can be further classified into three categories consistent with the arrangement of carrier signals: in-phase disposition (IPD), alternative phase opposite disposition (APOD), and phase opposite disposition (POD) [2]. However, the IPD method offers the lowest output voltage harmonics in comparison to other level-shifted modulations [19], thus it is employed in this study, as shown in Fig. 3. The modulation signal, which is generated based on the space vector pulse width modulation (SVPWM) technique specified as "T_a" shown in Fig. 3(a), is compared with triangular carrier waves that all have the same amplitude and frequency. The number of triangular carrier waves is determined by the CHB voltage levels, calculated as $(m-1)$; for example, the 5-level CHB inverter uses four triangular carrier waves, as illustrates in the figure based on the IPD approach.

The triangular carrier signals V_{cr1} and V_{cr1-} are used for the upper H-bridge cell to generate the pulse signals that activates switches S_{A11} and S_{A13}, respectively, as illustrated in Fig. 3(a) and Fig. 3(b). The switch S_{A11} will be activated when the modulation signal (Ta) is greater than or equal to $V_{cr1}(T_a \geq V_{cr1})$, as given in (4). Nonetheless, the switch S_{A13} is activated when the modulation signal is less than or equal to $V_{cr1}(T_a \leq V_{cr1-})$, as specified in (5) and shown in Fig. 3(b). Switches S_{A11} and S_{A12} are on the same inverter leg; hence, they are interlocked to each other, which cannot be activated

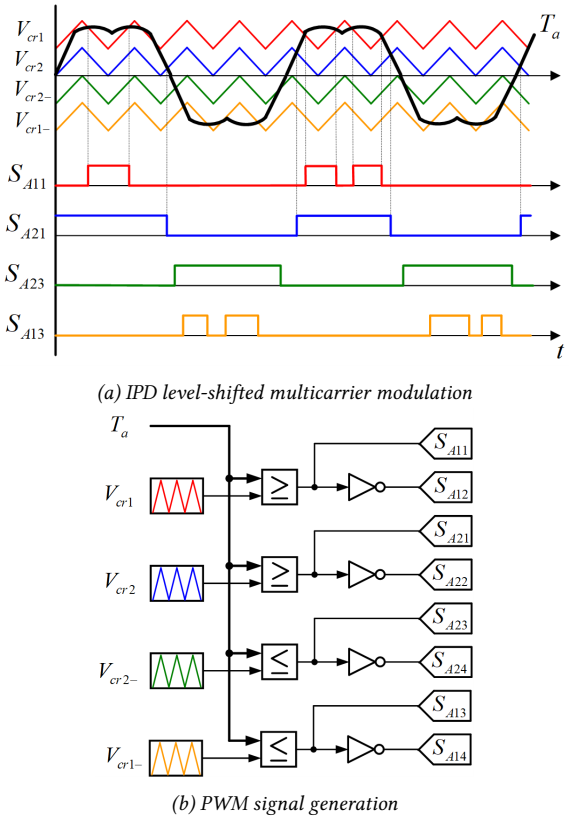

(a) IPD level-shifted multicarrier modulation

(b) PWM signal generation

***Fig. 3**: Switching Signal Generation for 5-level CHB Inverter Considering in Phase-A.*

together, and will be operated in the same way as other inverter legs. Similarly, the lower H-bridge cell uses V_{cr2} and V_{cr2-} for switches S_{A21} and S_{A23}, respectively. All gate signals defined in Fig. 3(b) are linked to switches in the 5-level CHB inverter depicted in Fig. 1(a).

$$S_{A11,A21} = \begin{cases} 1 & ; \quad T_a \geq V_{crx+} \\ 0 & ; \quad T_a < V_{crx+} \end{cases} \tag{4}$$

$$S_{A23,A13} = \begin{cases} 1 & ; \quad T_a \leq V_{crx-} \\ 0 & ; \quad T_a > V_{crx-} \end{cases} \tag{5}$$

where V_{crx+}, V_{crx-} denote triangular carrier signals on the positive and negative sides, respectively, and x presents a sequence number $(x = 1, 2)$.

3. CHB IM DRIVE SYSTEM

3.1 Mathematical Model of Induction Motors

Three-phase squirrel cage induction motors are widely utilized in various applications and have become crucial to industrial drives because of their advantages, for example, robustness, cost-effectiveness, reliability, simplicity, and low maintenance requirements [20], [21]. The d-axis and q-axis voltages in the synchronous reference frame, which is suitable for high-precision control of IM drives, are given by (6) and (7), respectively.

$$v_{ds} = R'_s i_{ds} + \sigma L_s \frac{di_{ds}}{dt} - \omega_e \sigma L_s i_{qs} - R_r \frac{L_m}{L_r^2} \psi_{dr} \tag{6}$$

$$v_{qs} = R'_s i_{qs} + \sigma L_s \frac{di_{qs}}{dt} + \omega_e \sigma L_s i_{ds} + \omega_r \frac{L_m}{L_r} \psi_{dr} \quad (7)$$

where v_{ds}, v_{qs} are d-axis and q-axis voltages, respectively, R'_s means stator transient resistance ($R'_s = R_s + R_r(L_m/L_r)^2$), i_{ds}, i_{qs} are d- and q-axis currents, respectively, σ is leakage coefficient ($\sigma = (1–(L_m^2/L_s L_r))$, R_r means rotor resistance, ω_e expresses an electric angular synchronous speed, L_s, L_r are stator and rotor inductances, respectively, L_m is mutual inductance, ω_r is the electrical angular speed of the rotor, and ψ_{dr} denotes the rotor flux of d-axis.

The induced torque can be determined by (8).

$$T_e = \frac{3}{2} \frac{L_m}{L_r} p \left(\psi_{dr} i_{qs} - \psi_{qr} i_{ds} \right) \quad (8)$$

where p denotes pole pairs, and ψ_{qr} means the rotor flux of q-axis.

The induced torque can be expressed by analyzing the mechanical components, as given by (9). It can be utilized to define the controller gains of the speed control loop for high-performance control strategy of IM drives.

$$T_e = J \frac{d\omega_{rm}}{dt} + B\omega_{rm} + T_L \quad (9)$$

where J, B mean moment of inertia and friction coefficient, respectively, ω_{rm} is the mechanical angular speed of the rotor, and T_L is the load-torque.

3.2 CHB-IM Control Strategy

Fig. 4 presents the rotor flux vector control diagram for IM drives that uses the field-oriented control (FOC) strategy operating with the 5-level CHB inverter. This method enables the independent control of rotor flux and torque by regulating the d-axis and q-axis currents, respectively [22]. The d-axis reference current, which is used to generate the rotor flux of the IMs, can be defined in (10). It is noted that since the IM utilizes the armature current to generate the rotor flux without the permanent magnets, the d-axis reference current would be set to a positive value based on the rated rotor flux. Meanwhile, the q-axis reference current is determined according to the speed control loop [23], as illustrated in the figure.

$$i^*_{ds} = \frac{\psi_{dr}}{L_m} \quad (10)$$

where $*$ indicates the reference value.

For the IMs, the slip angular speed is determined by utilizing motor parameters and armature currents given by (11). It is used to assess an electrical angular position in combination with the measured mechanical angular speed, as indicated in (12). Indeed, the electrical angular position is essential for the efficacy of the drive system employing the FOC method, as it confirms the accurate transformation of armature currents into the $d-q$ axis that aligned with the synchronous reference frame. Hence, the orthogonality of controlled currents on the $d-q$ axis can independently control the rotor flux and torque.

$$\omega_{sl} = \frac{R_r}{L_r} \frac{i_{qs}}{i_{ds}} \quad (11)$$

$$\theta_e = \int \left(\omega_{sl} + \omega_r \right) dt = \int \omega_e dt \quad (12)$$

where ω_{sl} is slip angular speed in rad/s, and θ_e denotes an electrical angular position.

The FOC approach uses proportional and integral (PI) current regulators in both d-axis and q-axis because they are dependable and uncomplicated controllers in vector control for AC drives [24]. The voltage equations in (6) and (7) are utilized to determine the PI regulator gains for the d-axis and q-axis current control loops, respectively. However, the last two parts of both voltage equations cannot be included in the transfer function of current control loops since there are cross-couplings and mutual voltages from the rotor flux to the stator voltage. Accordingly, the feedforward voltages are compensated to both d- and q-axes current control loops, as given by (13) and (14), respectively. It is also indicated in Fig. 4.

$$v_{dsc} = -\omega_e \sigma L_s i_{qs} - R_r \frac{L_m}{L_r^2} \psi_{dr} \quad (13)$$

$$v_{qsc} = \omega_e \sigma L_s i_{ds} + \omega_r \frac{L_m}{L_r} \psi_{dr} \quad (14)$$

The transfer functions that are employed to design the PI regulator gains for the $d-q$ axis currents and speed control loops are presented in equations (15)-(17) [24].

$$\frac{i_{ds}(s)}{i^*_{ds}(s)} = \frac{s k_{pcd} + k_{icd}}{s^2 \left(\sigma L_s \right) + s \left(R'_s + k_{pcd} \right) + k_{icd}} \quad (15)$$

$$\frac{i_{qs}(s)}{i^*_{qs}(s)} = \frac{s k_{pc,q} + k_{icq}}{s^2 \left(\sigma L_s \right) + s \left(R'_s + k_{pcq} \right) + k_{icq}} \quad (16)$$

$$\frac{\omega_m(s)}{\omega^*_m(s)} = \frac{\left(s k_{ps} + k_{is} \right) k_T}{s^2 J + s \left(B + k_{ps} k_T \right) + k_{is} k_T} \quad (17)$$

where s denotes a complex frequency domain in Laplace transform, k_{pcd}, k_{icd}, k_{pcq}, k_{icq} are regulator gains of the d- and q-axes current control loops, respectively, k_{ps}, k_{is} are regulator gains of the speed control loop, and k_T means the torque constant ($k_T = 1.5(L_m/L_r) \cdot p\psi_{dr}$).

4. SIMULATION RESULTS

A three-phase squirrel cage type IM with a power rating of 4.3 kW is utilized to demonstrate the impact of DC-link voltage fluctuation, resulting from the rectifier process, on the operation of the drive system. The FOC strategy with the CHB multilevel inverter is considered in the drive system, verified via the MATLAB/Simulink program. The SVPWM switching technique using the IPD level-shifted approach triggers the top and bottom H-bridge cells with a switching frequency of 4,500 Hz for the 5-level CHB inverter. Indeed, a single-phase AC

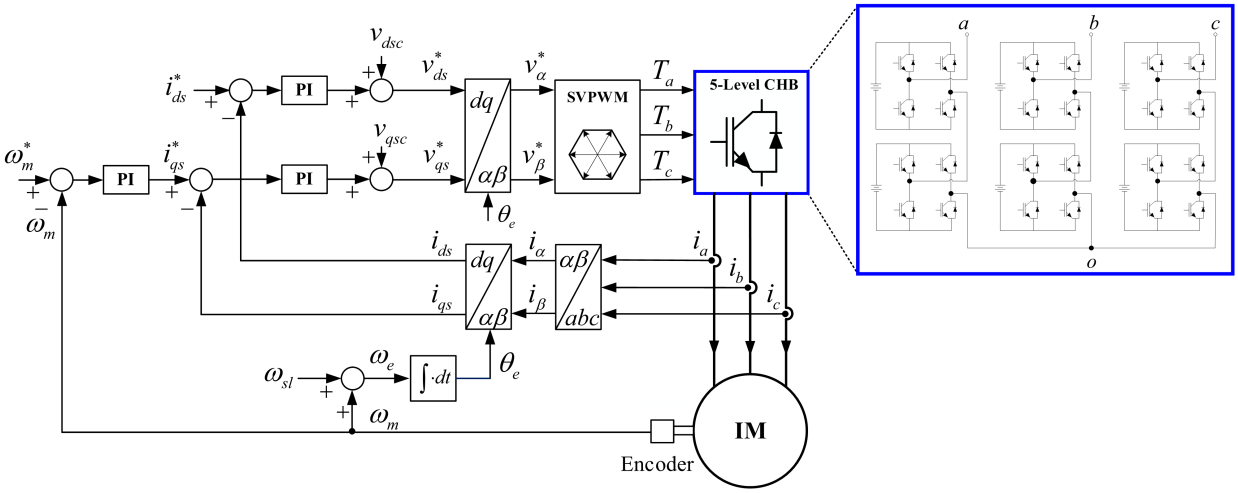

***Fig. 4**: Indirect Rotor Field Oriented Control Strategy of IM Drives Utilizing 5-level CHB Inverter.*

***Table 1**: Motor Parameters.*

Parameters	*Symbols*	*Values*
The rated torque	T_{rated}	28.3 *Nm*
Line voltage	V_L	380 V
Rated speed	ω_{rated}	1,450 *rpm*
Rated current	I_m	12.0 *A*
Armature winding resistance	R_s	0.711 *Ω*
Rotor winding resistance	R_r	0.441 *Ω*
Leakage inductance of stator	L_{ls}	3.209 *mH*
Leakage inductance of rotor	L_{lr}	4.594 *mH*
Mutual inductance	L_m	69.78 *mH*
Rated rotor flux	ψ_{dr}	0.4449 *Wb*
Moment of inertia	J	0.0138 $kg{\cdot}m^2$
Friction coefficient	B	0.000503 $Nm{\cdot}s$
Number of pole pairs	p	2
Leakage coefficient	σ	0.1030187

***Table 2**: Control Settings.*

Parameters	*Symbols*	*Values*
DC-link voltage of the CHB cell	V_{dc}	$110\sqrt{2}$ V
d-axis reference current	i_{ds}^*	6.3 *A*
Switching frequency	f_s	4,500 Hz
Bandwidth of current control loop	ω_{bc}	2827.433 rad/s
Bandwidth of speed control loop	ω_{bs}	282.743 rad/s
PI regulator gains of *d*- and *q*-axis current control loops	$k_{pc,d}$, $k_{pc,q}$	28.9672
	$k_{ic,d}$, $k_{ic,q}$	6112
PI regulator gains of speed control loop	k_{ps}	5.5176
	k_{is}	1103.2

supply is the main power source, used on the input side of all rectifiers. In order to clearly evaluate the influence of DC-link voltage ripple, the capacitance values of 100 μF, 1,000 μF, and 3,000 μF, which are utilized on the output side of rectifiers, are considered and compared with the ideal case. The motor parameters are indicated in Table 1. The *d*-axis reference current is set at 6.3 A, aligning with the rated rotor flux. All control settings for the 5-level CHB-IM drive are indicated in Table 2. The PI regulators of both current and speed control loops are designed based on the pole placement method since it offers fast dynamic response, good tracking accuracy, and high performance for AC drives [25].

The single-phase full bridge rectifier provides a DC source to the CHB inverter, while the capacitor typically stabilizes the output voltage; hence, varying capacitance values can make the ripples in the DC-link voltage more obvious. Fig. 5 shows the simulation results that validate the impact of DC-link voltage ripple on the 5-level CHB IM drive system. Fig. 5(a) shows the DC-link voltage waveforms produced by using capacitance values of 100 μF, 1,000 μF, and 3,000 μF with the rectifier of each H-bridge cell. The motor speed is steadily held at 500 rpm throughout the operating range, while the load torque is initially from no-load and transitions to 10.0 Nm at 0.4 s, as shown in Fig. 5(b). In the no-load conditions, the DC-link voltage stays smooth without any fluctuations across all cases of capacitance values, resulting in no torque ripple in this range (0 – 0.4 s), as shown in Fig. 5(b). Likewise, the *d*- and *q*-axes currents also remain constant without ripples, as shown in Fig. 5(c) and Fig. 5(d), respectively. The d-axis currents for all cases of capacitance values can track with the reference current, which is defined at 6.3 A, as given in Table 2. Meanwhile, the speed control loop provides the q-axis reference current, which will be zero under the no-load condition. It can be seen that a stable DC-link voltage can diminish both the torque ripple of the 5-level CHB IM drive under the no-load conditions and enable the motor speed to consistently follow its reference without variation, as illustrated in Fig. 6.

Under load conditions, load torque rapidly changes

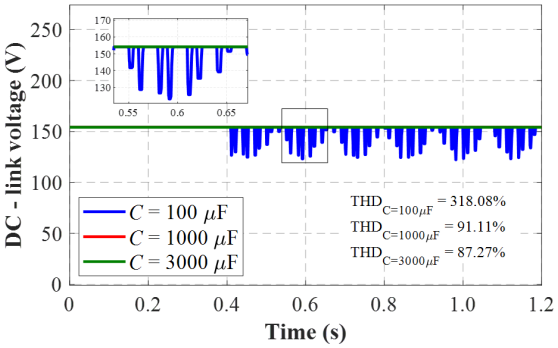

(a) DC-link voltage of a single H-bridge cell

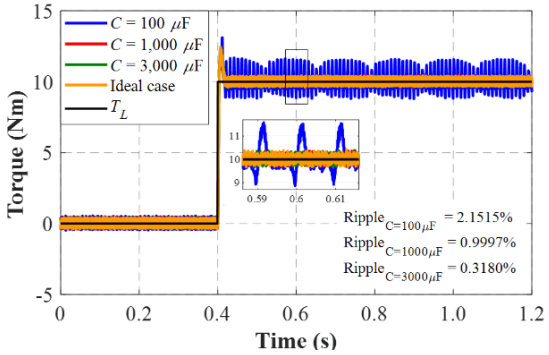

(b) Load torque

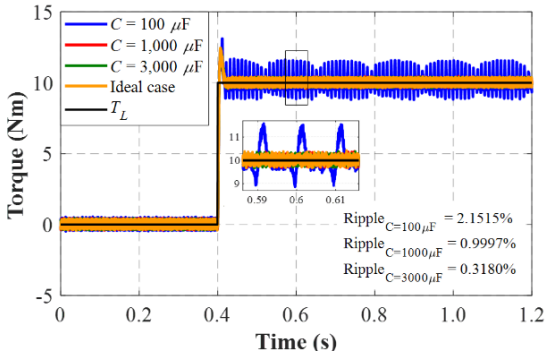

(c) d-axis current

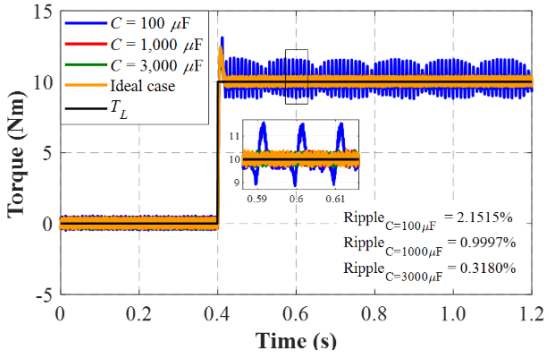

(d) q-axis current

***Fig. 5**: Simulation Results.*

from no load to 10.0 Nm at 0.4 s, consuming armature current around 10.5 A, whereas the speed is maintained at 500 rpm. The intrinsic voltage drop of rectifier units

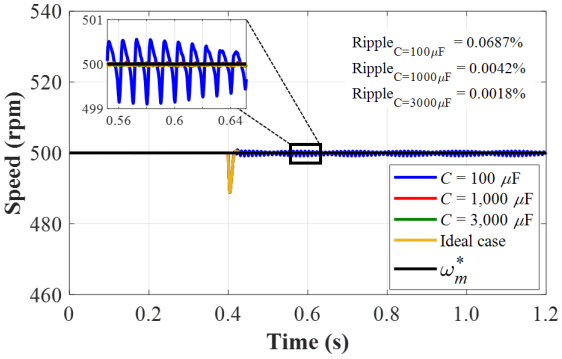

***Fig. 6**: Speed Ripple.*

would affect the characteristics of the DC-link voltage waveforms, as shown in Fig. 2(b). Indeed, the threshold voltage and internal resistance of both diode rectifiers and switches of the inverter are all set to 0.7 V and 0.02 Ω, respectively. The results show that employing a low capacitance value of 100 μF in the rectifier expresses 318.08% of the total harmonic distortion (THD), higher than capacitance values of 1,000 μF and 3,000 μF, which are 91.11% and 87.27%, respectively, leading to significantly greater fluctuations in the DC-link voltage, as demonstrated in Fig. 5(a). Likewise, the torque ripple harshens correspondingly as the DC-link voltage ripple increases, as shown in Fig. 5(b). In Fig. 5(b), the torque ripple for capacitance values of 100 μF, 1,000 μF, and 3,000 μF are approximately 2.15%, 0.99%, and 0.31%, respectively. High torque ripple is definitely not suitable for operating a motor drive system. The ripples of the DC-link voltage can impact not only the induced torque but also the motor speed, as can be clearly seen in Fig.6. Likewise, the d-q axis currents and motor speed exhibit considerable variations due to the obvious fluctuations in the DC-link voltage, as shown in Fig. 5(c), and Fig. 5(d), respectively. In contrast, minimal torque ripple is observed with capacitance values of 1,000 μF and 3,000 μF because of the low ripple in the DC-link voltage, which matches the d-q currents and motor speed. It should be noted that the PI regulators designed by the pole placement method of the 5-level CHB IM drive can offer good dynamic response and excellent tracking accuracy in both current and speed control loops, which can be seen in the tracking results in Figs. 5(c)-(d), and Fig. 6 for the d-q axis currents and speed, respectively.

The torque ripple can be determined by (18) [26], which is also applicable to the speed ripple.

$$T_{ripple} = \sqrt{\frac{1}{N}\sum_{k=1}^{N}\left(T_e(k) - T_{e,avg}\right)^2} \qquad (18)$$

where T_{ripple} represents torque ripple, N is the number of considered data, k is the number of considered points per cycle (where $k = 10,000$), and T_{avg} is the average torque.

It is worth noting that the capacitance values of 100

μF, 1,000 μF, and 3,000 μF are utilized only to illustrate the impact of ripples on the DC-link voltage waveforms generated by the single-phase full bridge rectifier. This study primarily examines the impact of variations in the DC-link voltage on the torque and speed ripples of the 5-level CHB IM drive based on the FOC strategy rather than concentrating on capacitor optimization. Although the impact of DC-link voltage ripple on the 5-level CHB IM drive has been illustrated through simulations, the resultant torque ripple and variations in motor speed can greatly influence the performance of the drive system, contingent upon the quality of the DC-link voltage waveform that should be taken into account.

5. CONCLUSION

This study examines the impact of DC-link voltage ripple on the performance of the 5-level CHB IM drive, especially in terms of torque ripple and speed variations. A single-phase full bridge rectifier is used to generate a DC source for each H-bridge cell; therefore, capacitance values of 100 μF, 1,000 μF, and 3,000 μF are utilized to demonstrate the different amounts of ripple in the DC-link voltage clearly. In this validation, the motor speed is consistently held at 500 rpm throughout the operating range, whereas the load torque is considered in both no-load and with-load (10.0 Nm) conditions. The results indicate that the DC-link voltage stays smooth without any fluctuations across all cases of capacitance values in the no-load condition, leading to the absence of torque ripple and motor speed variations. Nevertheless, under load conditions, the DC-link voltage exhibits increased fluctuations when a low capacitance value of 100 μF is utilized in comparison to other capacitance values. As a result, the torque and motor speed exhibit considerable variations. Consequently, evaluating the quality of the DC-link voltage waveform is essential since it directly impacts the performance of the drive system.

ACKNOWLEDGEMENT

This research was supported by University of Phayao and Thailand Science Research and Innovation Fund (Fundamental Fund 2025)

REFERENCES

[1] Z. Ni, A. H. Abuelnaga, and M. Narimani, "A New Fault-Tolerant Technique Based on Nonsymmetrical Selective Harmonic Elimination for Cascaded H-Bridge Motor Drives," *IEEE Transactions on Industrial Electronics*, vol. 68, no. 6, pp. 4610-4622, June 2021.

[2] B. Wu and M. Narimani. *High Power Converters and AC Drives*, 2nd ed. New York: John Wiley and Sons, 2017.

[3] H. Yao, Y. Yan, Y. Cao, P. Song, and T. Shi, "A Variable Duty Cycle-Based Predictive Control for PMSM Fed by Cascaded H-Bridge Inverter," *IEEE Journal of Emerging and Selected Topics in Power Electronics*, vol. 10, no. 4, pp. 4195-4206, Aug. 2022.

[4] P. S. Jamwal, S. Singh, and S. Jain, "Three-Level Inverters for Induction Motor Driven Electric Vehicles," in *2021 3rd International Conference on Energy, Power and Environment: Towards Clean Energy Technologies*, Shillong, Meghalaya, India, 2021, pp. 1-6.

[5] N. A. Rahim, M. F. M. Elias, and W. P. Hew, "Transistor-Clamped H-Bridge Based Cascaded Multilevel Inverter with New Method of Capacitor Voltage Balancing," *IEEE Transactions on Industrial Electronics*, vol. 60, no. 8, pp. 2943-2956, Aug. 2013.

[6] P. Kant and B. Singh, "Multiwinding Transformer Fed CHB Inverter with On-Line Switching Angle Calculation Based SHE Technique for Vector Controlled Induction Motor Drive," *IEEE Transactions on Industry Applications*, vol. 56, no. 3, pp. 2807-2815, May-June 2020.

[7] G. Pongnot, A. Desreveaux, C. Mayet, D. Labrousse, and F. Roy, "Comparative Analysis of a Low-Voltage CHB Inverter Without PWM and Two-Level IGBT/SiC Inverters for Electric Vehicles on Driving Cycles," *IEEE Open Journal of Vehicular Technology*, vol. 6, pp. 542-553, Jan. 2025.

[8] D. Kang, S. Badawi, Z. Ni, A. H. Abuelnaga, M. Narimani, and N. R. Zargari, "Review of Reduced Switch-Count Power Cells for Regenerative Cascaded H-Bridge Motor Drives," *IEEE Access*, vol. 10, pp. 82944-82963, Aug. 2022.

[9] M. A. Tariq and S. A. Rahman Kashif, "Impact of the Voltage Profiles of CHB vs MW-Type Inverters on Torque and Speed Ripples for 3-Phase Induction Motors," in *2024 IEEE Workshop on Control and Modeling for Power Electronics (COMPEL)*, Lahore, Pakistan, 2024, pp. 1-7.

[10] F. Khoucha, S. M. Lagoun, K. Marouani, A. Kheloui, and M. E. H. Benbouzid, "Hybrid Cascaded H-Bridge Multilevel-Inverter Induction-Motor-Drive Direct Torque Control for Automotive Applications," *IEEE Transactions on Industrial Electronics*, vol. 57, no. 3, pp. 892-899, Mar. 2010.

[11] Q. Sun et al., "Reconsideration on Capacitor Ripple Voltage of CHB-StatCom: Observation, Modeling, Analysis, and Application of Ripple Effect from Design Perspective," *IEEE Transactions on Power Electronics*, vol. 37, no. 11, pp. 13626-13640, Nov. 2022.

[12] Z. Ni, A. Abuelnaga, M. Narimani, and N. R. Zargari, "DC-Link Voltage Ripple Control of Regenerative CHB Drives for Capacitance Reduction," *IEEE Transactions on Industrial Electronics*, vol. 69, no. 4, pp. 3245-3254, Apr. 2022.

[13] A. H. Abuelnaga, Z. Ni, S. Badawi, M. Narimani, A. Sayed-Ahmed, and N. R. Zargari, "A New Active Front-End Control for Regenerative Cascaded H-Bridge Motor Drives with Filter-Less Interfacing Capability," *IEEE Transactions on Power Electronics*,

vol. 38, no. 7, pp. 8559-8570, Jul. 2023.

[14] Q. Song, W. Yang, B. Zhao, J. Meng, S. Xu and Z. Zhu, "Low-Capacitance Modular Multilevel Converter Operating with High Capacitor Voltage Ripples," *IEEE Transactions on Industrial Electronics*, vol. 66, no. 10, pp. 7456-7467, Oct. 2019.

[15] D. Kang et al., "A Reduced Switch Count Power Cell for Regenerative Cascaded H-Bridge (CHB) Converter," *IEEE Access*, vol. 12, pp. 161453-161467, Oct. 2024.

[16] J. Shen, S. Schröder, J. Gao, and B. Qu, "Impact of DC-Link Voltage Ripples on the Machine-Side Performance in NPC H-Bridge Topology," *IEEE Transactions on Industry Applications*, vol. 52, no. 4, pp. 3212-3223, Jul.-Aug. 2016.

[17] Y. Zhang, Z. Li, F. Gao, C. Zhao, H. Zhang, and Y. Li, "Analysis of DC-Link Voltage Fluctuations in CHB Inverter with Supercapacitor and DC–DC Stage Under Hybrid Modulation Strategy," in *2024 10th IEEE International Power Electronics and Motion Control Conference (IPEMC2024-ECCE Asia)*, Chengdu, China, 2024, pp. 2184-2188.

[18] A. Poorfakhraei, M. Narimani and A. Emadi, "A Review of Modulation and Control Techniques for Multilevel Inverters in Traction Applications," *IEEE Access*, vol. 9, pp. 24187-24204, Feb. 2021.

[19] [19] M. Angulo, P. Lezana, S. Kouro, J. Rodriguez, and B. Wu, "Level-Shifted PWM for Cascaded Multilevel Inverters with Even Power Distribution," in *2007 IEEE Power Electronics Specialists Conference*, Orlando, FL, USA, 2007, pp. 2373-2378.

[20] S. S. Choi, M. -H. Yoon, C. M. Park, and S. H. Lim, "Analysis on Arcing Reduction due to Driving Operation of Induction Motor through Application of SFCL in a Power Distribution System," *IEEE Transactions on Applied Superconductivity*, vol. 35, no. 5, pp. 1-5, Aug. 2025.

[21] G. Abad. Narimani. *Power Electronics and Electric Drives for Traction Applications*, 1st ed. New York: John Wiley and Sons, 2017.

[22] S. M. Yang and K. W. Lin, "Automatic Control Loop Tuning for Permanent-Magnet AC Servo Motor Drives," *IEEE Transaction on Industrial Electronics*, vol. 63, no. 3, pp. 1499-1506, Mar. 2016.

[23] F. Mendoza-Mondragón, V. M. Hernández-Guzmán, and J. Rodríguez-Reséndiz, "Robust Speed Control of Permanent Magnet Synchronous Motors Using Two-Degrees-of-Freedom Control," *IEEE Transaction on Industrial Electronics*, vol. 65, no. 8, pp. 6099-6108, Aug. 2018.

[24] S. H. Kim. *Control of Direct Current Motors, in Electric Motor Control DC, AC, and BLDC Motors*, 1st ed. Cambridge: Elsevier, 2017.

[25] P. Kaewma, N. Pothi, and C. Rakpenthai, "Dynamic Response Analysis of Induction Motor Drive Influenced by Controller Design Methods," *International Journal of Power Electronics and Drive Systems (IJPEDS)*, vol. 16, no. 1, pp. 129-137, Mar. 2025.

[26] D. Mohan, X. Zhang and G. H. Beng Foo, "Generalized DTC Strategy for Multilevel Inverter Fed IPMSMs with Constant Inverter Switching Frequency and Reduced Torque Ripples," *IEEE Transactions on Energy Conversion*, vol. 32, no. 3, pp. 1031-1041, Sep. 2017.

Adisorn Jewsubpong received the B.Eng degree in electrical engineering from University of Phayao, Thailand, in 2022. He is currently studying toward M.Eng degree in electrical engineering from University of Phayao. His research interests include the areas of multilevel inverter applications and electric motor drives.

Nattapong Pothi received the B.Eng. and M.Eng. degrees both in electrical engineering from Chiang Mai university, Thailand, in 2003 and 2007, respectively, and Ph.D. degree in electronic and electrical engineering from University of Sheffield, Sheffield, U.K., in 2016. Since 2007, he has been with the school of Engineering, University of Phayao, Thailand, where he is currently an Assistant Professor in the Department of Electrical Engineering. His research interests include the areas of electric motor drives, flux-weakening control, energy conversion systems, and power electronic applications.

Chawasak Rakpenthai received the B.Eng., M.Eng., and Ph.D. degrees in electrical engineering from Chiang Mai University, Thailand, in 1999, 2003, and 2007, respectively. He is currently a Professor at the Department of Electrical Engineering, University of Phayao. His research interests include applications of artificial intelligence in power system, power electronics, power system state estimation, and FACTS devices.

Jonglak Pahasa received the B.Eng. degree from the King Mongkut's Institute of Technology Ladkrabang (KMITL), Bangkok, Thailand, in 1997, the M.Eng. degree from Chiang Mai University, Chiang Mai, Thailand, in 2007, and the D.Eng. degree from KMITL in 2011 all in electrical engineering. She is currently an Assistant Professor with the School of Engineering, University of Phayao, Phayao, Thailand. Her current research interests include the applications of artificial intelligence in power system stability and control.